

## Article

# Impact of Modifier Oxides on Mechanical and Radiation Shielding Properties of B<sub>2</sub>O<sub>3</sub>-SrO-TeO<sub>2</sub>-RO Glasses (Where RO = TiO<sub>2</sub>, ZnO, BaO, and PbO)

M. I. Sayyed <sup>1,2,\*</sup> , M. Kh. Hamad <sup>3,\*</sup> , Mohammad Hasan Abu Mhareb <sup>4,5</sup> , K. A. Naseer <sup>6</sup> , K. A. Mahmoud <sup>7,8</sup> ,  
Mayeen Uddin Khandaker <sup>9</sup> , Hamid Osman <sup>10</sup>  and Basem H. Elesawy <sup>11</sup>

- <sup>1</sup> Department of Physics, Faculty of Science, Isra University, Amman 11622, Jordan
  - <sup>2</sup> Department of Nuclear Medicine Research, Institute for Research and Medical Consultations (IRMC), Imam Abdulrahman bin Faisal University (IAU), Dammam 31441, Saudi Arabia
  - <sup>3</sup> Department of Basic Sciences, School of Social and Basics Sciences, Al Hussein Technical University, King Abdullah II St 242, Amman 11831, Jordan
  - <sup>4</sup> Department of Physics, College of Science, Imam Abdulrahman Bin Faisal University, Dammam 31441, Saudi Arabia; mhsabumhareb@iau.edu.sa
  - <sup>5</sup> Basic and Applied Scientific Research Center, Imam Abdulrahman Bin Faisal University, Dammam 31441, Saudi Arabia
  - <sup>6</sup> Department of Physics, The Gandhigram Rural Institute-Deemed to be University, Gandhigram 624302, India; naseerka.phy6@gmail.com
  - <sup>7</sup> Department of Nuclear Power Plants and Renewable Energy Sources, Ural Power Engineering Institute, Ural Federal University, St. Mira 19, 620002 Yekaterinburg, Russia; karemadbelazeem@yahoo.com
  - <sup>8</sup> Nuclear Materials Authority, El-Maadi, Cairo P.O. Box 530, Egypt
  - <sup>9</sup> Center for Applied Physics and Radiation Technologies, School of Engineering and Technology, Sunway University, Bandar Sunway 47500, Malaysia; mayeenk@sunway.edu.my
  - <sup>10</sup> Department of Radiological Sciences, College of Applied Medical Sciences, Taif University, Taif 21944, Saudi Arabia; ha.osman@tu.edu.sa
  - <sup>11</sup> Department of Pathology, College of Medicine, Taif University, Taif 21944, Saudi Arabia; b.elesawy@tu.edu.sa
- \* Correspondence: dr.mabualssayed@gmail.com (M.I.S.); hamad\_morad85@yahoo.com (M.K.H.)



**Citation:** Sayyed, M.I.; Hamad, M.K.; Abu Mhareb, M.H.; Naseer, K.A.; Mahmoud, K.A.; Khandaker, M.U.; Osman, H.; Elesawy, B.H. Impact of Modifier Oxides on Mechanical and Radiation Shielding Properties of B<sub>2</sub>O<sub>3</sub>-SrO-TeO<sub>2</sub>-RO Glasses (Where RO = TiO<sub>2</sub>, ZnO, BaO, and PbO). *Appl. Sci.* **2021**, *11*, 10904. <https://doi.org/10.3390/app112210904>

Academic Editor:  
Abilio M. P. De Jesus

Received: 12 October 2021  
Accepted: 10 November 2021  
Published: 18 November 2021

**Publisher's Note:** MDPI stays neutral with regard to jurisdictional claims in published maps and institutional affiliations.



**Copyright:** © 2021 by the authors. Licensee MDPI, Basel, Switzerland. This article is an open access article distributed under the terms and conditions of the Creative Commons Attribution (CC BY) license (<https://creativecommons.org/licenses/by/4.0/>).

**Abstract:** The influence of modifier oxides (TiO<sub>2</sub>, ZnO, BaO, and PbO) on the mechanical and radiation shielding properties of boro-tellurate glasses is investigated. Samples with a composition of B<sub>2</sub>O<sub>3</sub>-SrO-TeO<sub>2</sub>-RO (RO represents the modifier oxides) were fabricated using the melt quench method, and their physical, mechanical, and radiation attenuation parameters were reported. For this aim, Monte Carlo simulation was employed to predict the radiation attenuation parameters, while the Makishima-Mackenzie model was adopted to determine the mechanical properties. The tightly packed structure with better cross-linkage density is possessed by the Ti-containing glass (SBT-Ti) system among the titled glass batch. The higher Poisson and micro-hardness values of the SBT-Ti glass indicate its structure's reduced free volume and better compactness. For the glass with PbO, the linear and mass attenuation coefficients are highly increased compared to those glasses doped with TiO<sub>2</sub>, ZnO, and BaO. The thinner half-value layer was reported at 0.015 MeV, taking values 0.006, 0.005, 0.004, and 0.002 for samples with TiO<sub>2</sub>, ZnO, BaO, and PbO, respectively. SBT-Pb sample (with PbO) has a thinner HVL compared to other fabricated glass samples. The fabricated glasses' thickness (Deq) equivalent to 1 cm of lead (Pb) was reported. The results demonstrated that Deq is high at low energy and equals 11.62, 8.81, 7.61, 4.56 cm for SBT-Ti, SBT-Zn, SBT-Ba, and SBT-Pb glass samples, respectively. According to the Deq results, the fabricated glasses have a shielding capacity between 30 and 43% compared to the pure Pb at gamma-ray energy of 1.5 MeV. At high energy (8 MeV), the transmission factor values for a thickness of 1 cm of the fabricated samples reach 88.68, 87.83, 85.95, and 83.11% for glasses SBT-Ti, SBT-Zn, SBT-Ba, and SBT-Pb, respectively.

**Keywords:** radiation shielding; monte carlo simulation; melt-quench technique; mechanical properties

## 1. Introduction

Reasoned from industrialization, a ton of energy is delivered due to the increase in nuclear power plants. Making energy requires the lower cost of each crude material engaged with the cycle. The materials utilized for radiation shielding are indispensable and, subsequently, can't think twice about quality. In this way, the best way to decrease the expense is to discover new materials that can give better wellbeing for a minimal price. This is the motivation behind why a lot of exploration is going on around the world in regard to the safeguarding properties of different materials [1–8].

Nowadays, a great interest is awarded by analysts to track down an appropriate elective contender for radiation protecting implementations. They understood that the glass systems could be favorable substances to obstruct harmful radiation. The ease of fabrication of glass, the transparency for light, and the simple design make the attractive environment for researchers [9,10]. Various research groups are presently exploring the optically translucent glasses that can safeguard these radioactive beams adequately. In any case, the host network's decision is vital for glass structure in attainable temperature with excellent transparency. Likewise, to have the protecting properties, it is in every case great to pick a host with heavy metal oxides (HMO) [11]. Therefore, metal oxides like  $\text{SiO}_2$ ,  $\text{TeO}_2$ ,  $\text{PbO}$ ,  $\text{BaO}$ ,  $\text{ZnO}$ , and  $\text{Bi}_2\text{O}_3$ , etc., could be used for practical applications. The fabrication, transport, and cleaning of glasses are so easy that led to various tries for studying the effect of different constituents on glass structures. The glasses have erosion obstruction, could be financially viable and transparent, which is a one-of-a-kind trademark. They have several advantages, and they can be utilized as a protecting substance and store container for nuclear garbage. Similarly, for the reasonable treatment of the dangerous beams, it is essential to have information about the photon interaction parameters (PIP) [12].

Among the various conceivable host matrices, conditional glass former tellurite ( $\text{TeO}_2$ ) and the conventional glass former borate ( $\text{B}_2\text{O}_3$ ) based glasses are alluring hosts because of their particular trademark highlights. The use of  $\text{TeO}_2$  with  $\text{B}_2\text{O}_3$  led to reducing the hygroscopic properties for borate and increasing the durability of the glass matrix, and this result can be seen in the previous work [13,14]. Among the few glasses framing oxides, there is a broad measure of revenue in the choice of borate-based glass as the host lattice for the radiation protecting applications due to their surprising physical, mechanical, structural, and optical properties like transparency, lower dissolving temperature, and higher dielectric constant regardless of the way that they have more considerable phonon energy [15,16]. Further, it is more fascinating because of its unconventional "boron anomaly" conduct. By adding alkaline earth metals such as  $\text{Ba}^{2+}$ ,  $\text{Ca}^{2+}$  into the network, one can catalyze the alteration of trigonal borates ( $\text{BO}_3$ ) to tetrahedron borates ( $\text{BO}_4$ ) which enhances the quantity of non-bridging oxygens (NBOs). The NBOs enhance various structural properties of the glasses. Furthermore, different research groups show tremendous interest in  $\text{TeO}_2$  based glasses because of their benefits, which incorporate elevated density, better transparency in the mid-infrared region, reasonable phonon energy, superior mechanical and chemical constancy, etc., which make them a possible contender for the creation of optoelectronic gadgets [17]. Besides, the presence of Zinc oxide ( $\text{ZnO}$ ) in the picked glass framework works on the mechanical potency, chemical firmness and inferior thermal expansion, hygroscopic character.  $\text{ZnO}$  is a fantastic option for giving steadiness for the borate glasses for a minimal price. Additionally, the non-toxic nature makes it an eco-accommodating factor [18]. The glass-forming chance may likewise be improved with the introduction of  $\text{ZnO}$  by the change of fundamental  $\text{TeO}_4$  units. Furthermore, it is relied upon to abbreviate the ideal opportunity for hardening during the quenching process. The alkali earth ions increment the chemical soundness and diminish the most extreme phonon energy through the progressive switch of  $\text{BO}_3 \leftrightarrow \text{BO}_4$  and  $\text{TeO}_3 \leftrightarrow \text{TeO}_4$  [19]. Also, barium oxide ( $\text{BaO}$ ) is utilized in glass systems as a modifier; the purpose of using  $\text{BaO}$  lies in improving density and stability for different glass systems [20]. While titanium oxide ( $\text{TiO}_2$ ) can protect optical efficiency for glass systems when used within percent less than 20% [20], this percent was applied in this work. The addition of lead oxide ( $\text{PbO}$ ) to various

glass formers results in an extensive glass formation range of 20–80% and an adjustable refractive index [21].

The current work is designed to evaluate various mechanical features and the radiation shielding potency of boro-tellurate glasses by changing the modifying HMO.

## 2. Materials and Methods

### 2.1. Glass Fabrication

Seven oxides like strontium oxide (SrO), tellurium oxide (TeO<sub>2</sub>), boron oxide (B<sub>2</sub>O<sub>3</sub>), titanium oxide (TiO<sub>2</sub>), zinc oxide (ZnO), barium oxide (BaO), and lead oxide (PbO) were utilized to fabricate four glass samples using the traditional melt-quench technique. The oxides were purchased from different company: SrO (99.9%), TeO<sub>2</sub> (98%), B<sub>2</sub>O<sub>3</sub> (98%), BaO (99%) and (PbO) Aldrich, and ZnO (99.9%) WINLAB, while TiO<sub>2</sub> (98%) from BDH chemical Ltd. No purification was used for these chemicals. The chemical ratios for oxides are enlisted in Table 1. The traditional melt quench method was started by weighting the oxides carefully based on the mole percent for each sample, as shown in Table 1. After that, these chemical oxides were mixed and put in an alumina crucible. The mixture was introduced in an electrical furnace at 1000 °C for 30 min to perform the melting process, and the mixture was stirred periodically during the melting process. Subsequently, the crucible was poured on a steel plate inside another furnace at 400 °C to form glasses. The glasses were kept inside the electrical furnace for three hours to minimize the stress and reduce the glass fracture probability; then, the furnace temperature was lowered with a cooling rate of 15 °C/min.

**Table 1.** The composition and density of the prepared glasses.

Sample Codes	Composition Ratios (mol%)							Density (g/cm <sup>3</sup> )
	SrO	B <sub>2</sub> O <sub>3</sub>	TeO <sub>2</sub>	TiO <sub>2</sub>	ZnO	BaO	PbO	
SBT-Ti	10	35	35	20	0	0	0	4.0591
SBT-Zn	10	35	35	0	20	0	0	4.2968
SBT-Ba	10	35	35	0	0	20	0	4.7395
SBT-Pb	10	35	35	0	0	0	20	5.2657

The density for current glasses was measured experimentally using Archimedes principle; the special density kit from Rad Wag company was employed for determining the sample weight in the air (*A*) and liquid (*B*) according to the next relation:

$$\rho = \frac{A}{A - B} x \rho_{liq} \quad (1)$$

Here,  $\rho_{liq}$  represents the water density utilized as an immersion fluid in this experiment, this method was utilized in our previous work [22,23].

### 2.2. Mechanical Properties Calculations

Makishima and Mackenzie's calculation method was adopted for evaluating the mechanical properties of the prepared samples [24,25]. The following are the semi-empirical equations for estimating the dissociation energy ( $G_t$ ), packing density ( $V_t$ ), elastic moduli, and Poisson's ratio of the prepared glasses.

Dissociation energy

$$G_t = \sum_i x_i G_i \quad (2)$$

Packing density

$$V_t = \frac{\rho}{M} \sum_i x_i V_i \quad (3)$$

where in,  $G_i$  = dissociation energy per unit volume and  $V_i$  = packing density with the *i*th components calculated from the literature [26].

$$\text{Young's modulus} \quad E = 8.36 V_t G_t \quad (4)$$

$$\text{Bulk modulus} \quad K = 10.00 V_t^2 G_t \quad (5)$$

$$\text{Shear modulus} \quad S = 3K / (10.2V_t - 1) \quad (6)$$

$$\text{Longitudinal modulus} \quad L = K + \frac{4}{3} S \quad (7)$$

$$\text{Poisson's ratio} \quad \mu = 0.5 - (1/7.2V_t) \quad (8)$$

$$\text{Hardness} \quad H = \frac{1 - 2\mu}{6(1 + \mu)} \quad (9)$$

The elastic moduli are expressed in terms of glass composition,  $G_t$ , and  $V_t$ .

### 2.3. Radiation Shielding Calculations Using Monte Carlo Simulation

It is known that the Monte Carlo simulation is a non-destructive method used to predict the shielding parameters of any material. The Monte Carlo simulation is a practical, non-expensive method that can save time and protect persons from the hazards of the radioactive sources during the experimental measurements. Also, in recent years many articles reported agreement between the simulated results predicted by the Monte Carlo simulations and the experimental measurements [27,28]. In the present, the Monte Carlo simulation was utilized to predict the shielding parameters in the energy range between 0.015 and 15 MeV for some tellurite-based glasses. The chemical composition and density of the fabricated glasses presented in Table 1 were utilized in the MC simulation input file to introduce the fabricated material. The input file also introduces the dimensions of the sample where it is a cylinder with a diameter of 1 cm and a thickness of 0.25 cm. The sample was placed with a distance of 9 cm from the detector and 11 cm from the point source. Also, the sample is placed between two collimators to collimate the radiation emitted from the radioactive source and transmitted from the sample. These two collimators as well as the outer shielding material (the outer cylinder), are made of lead with dimensions illustrated in Figure 1. The detector in the present study is an F4 tally to record the detector cell's mean flux per unit volume. The simulation carried out with NPS card equal  $10^6$  historical, and the importance is assumed to be 1 for important cells (cells in which the photons can pass and interact) and 0 for void cells (cells in which the photons shouldn't pass). The source card is arranged in the input file to describe the radioactive source location, emission type, direction of emission, energy, probability, and distribution of the emitted particle. The simulation was performed, and the output files showed that the relative error was in the range of  $\pm 1\%$ . Finally, the received average track length for all samples was transferred to other linear attenuation coefficients.

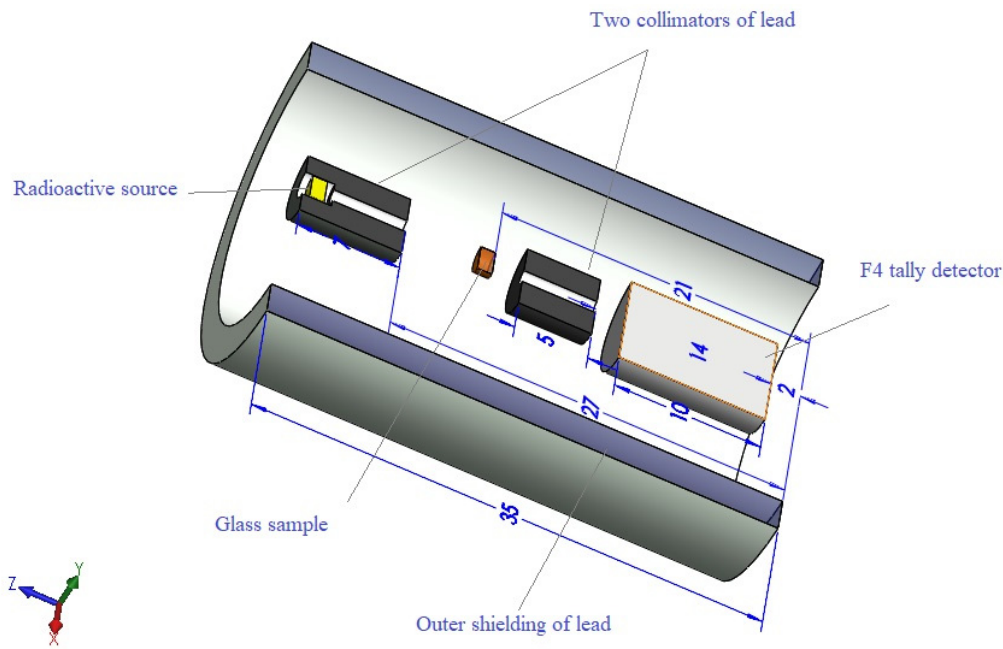


**Figure 1.** The created geometry describes the Monte Carlo simulation input file.

### 3. Result and Discussion

#### 3.1. Material Features Study

The application of glassy complexes for radiation shielding purposes is a function of its composition, which accordingly impacts the material properties of the system. Following the proposed glass’s compositional layout, some physical and mechanical attributes were computed to depict the effect of various heavy metal ion modifiers incorporated in the system. From Tables 1 and 2, the variation in the measured density and molar volume values validate the effect of modifiers, and it is graphically signified in Figure 2. The figure indicates the compositional variation in density and molar volume as the additive is varied in each system and the values follow the order SBT-Pb > SBT-Ba > SBT-Zn > SBT-Ti and SBT-Ti > SBT-SBT-Pb > SBT-Ba > SBT-Zn, respectively. The behavior of molar volume is contrary to that of density in the general case. However, in the current investigation, it is unnoticed due to the formation of various structural units due to additives inclusion and non-bridging oxygens (NBOs) creation in the modifier reliant multi-component glass matrices [29].

**Table 2.** Physical and mechanical attributes of the prepared glasses.

	SBT-Ti	SBT-Zn	SBT-Ba	SBT-Pb
MW	106.561	106.864	121.253	135.228
Molar volume	26.252	24.871	25.584	25.681
$V_i$	16.405	15.065	15.285	15.825
$G_t$	72.660	62.400	60.320	57.480
$V_t$	0.625	0.606	0.597	0.616
Young	90.810	75.596	72.077	70.840
Bulk	68.096	54.949	51.675	52.384
Shear	35.535	29.746	28.432	27.789
Poisson	0.278	0.271	0.268	0.275
micro-hardness	5.265	4.547	4.406	4.176
Longitudinal	115.476	94.610	89.585	89.436
longitudinal velocity	5333.739	4692.414	4347.607	4121.235
Shear velocity	2958.797	2631.106	2449.274	2297.251
Softening temperature	452.948	339.322	302.472	267.102
Bond fractal conductivity	2.087	2.165	2.201	2.122

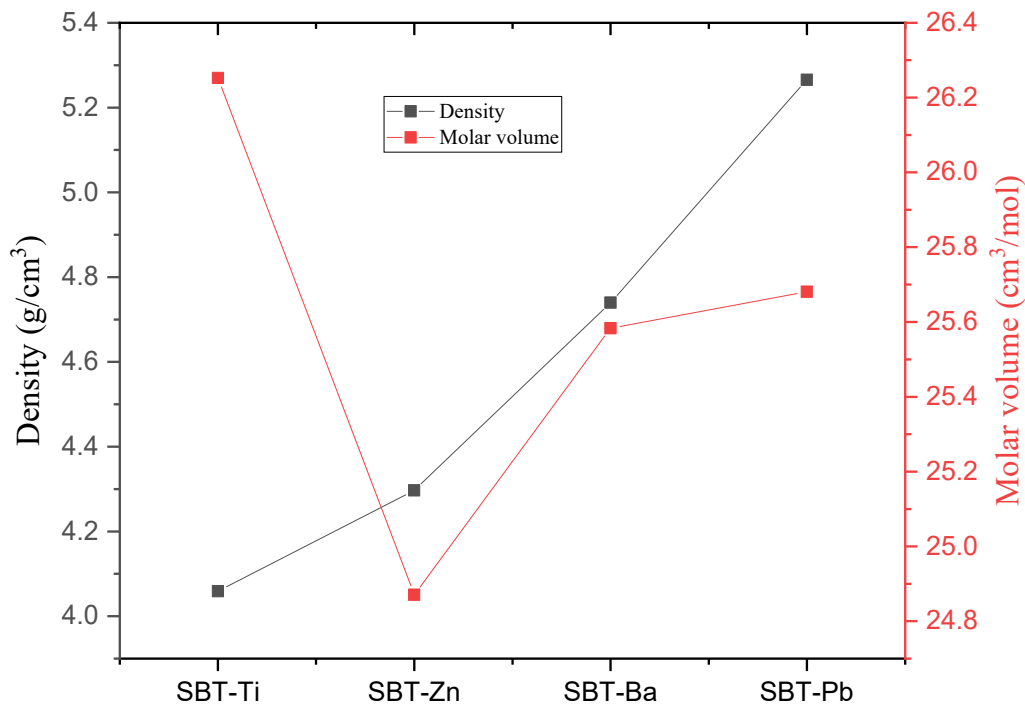


**Figure 2.** The correlation between density and molar volume of the fabricated SBT glasses.

In the case of multi constituent glasses, each element applies its effect so that any change in the mechanical attribute can be considered as a combination of the impact of all the individual constituents. With this context, the mechanical moduli (including young, bulk, shear, and longitudinal moduli) along with Poisson's ratio, microhardness, and more features were calculated for the as-prepared glass specimens with the formulae specified in the literature [26,30] and gathered in Table 2. The correlation between dissociation energy and packing density is illustrated in Figure 3, which depicts the fact that among all the proposed glasses, SBT-Ti is noticed to own greater volume density of binding energy and reduced ionic volume that are essential for better radiation attenuation. The structural compactness and alteration in the geometrical arrangement in the glass complexes due to additives inclusion are apparent from the estimated elastic constants, which are graphically correlated in Figure 4. The change in the elastic moduli denotes the distinction in the nature and strength of the chemical bonds, cross-link density, which describes the glass configuration and is also related to the dissociation energy of the system. Figure 4 proves that the tightly packed structure with better cross-linkage density is possessed by the SBT-Ti glass system among the titled glass batch. The elastic moduli also rely on the shear and longitudinal velocities of the complex, which are also high for the SBT-Ti glass system, as observed in Table 2. The gradual reduction in both the velocities in the systems with different additives results from the rise in the molar volume, which leads to a loosened structure [31].

Commonly, the Poisson's ratio of glassy complexes is affected by the alteration in its cross-link density which arises from the structural modification [20,32]. If the Poisson's ratio lies in the range 0.1–0.2, the cross-link density will be high for the system with the better tightly packed structure to capture radiation [32]. For the present proposed glasses, the Poisson's ratio lies in the range 0.268–0.278, depicting better cross-link density of the tiled glasses that signifies better shielding performance. From the table, the observed reduction in the softening temperature (SBT-Ti > SBT-Zn > SBT-Ba > SBT-Pb) denotes the rise in the production of NBO that causes a loosely bounded glass structure with reduced lattice vibrations. The micro-hardness usually depicts the essential stress to remove the glass matrix's free volume (distortion of the system) [33]. The free volume denotes the loosely

packed structure, which should be minimum for a shielding medium. Figure 5 portrays the correlation between Poisson and micro-hardness of the studied glasses that expresses higher values of the SBT-Ti glass, indicating reduced free volume and better compactness of the structure than other samples. The bond fractal connectivity is a vital feature relating the mechanical attributes of glasses to their networks. The effective dimensionality and cross-link density of glassy systems can be expressed by means of bond fractal connectivity. The evaluated values may lie in the range of 1,2,3 for the chain, layer structure, and 3D structure depending upon the complexes. It is apparent from Table 2 that the assessed values lie in the range 2.087–2.201 for the as-polished samples symbolizing their 2D layer structure.

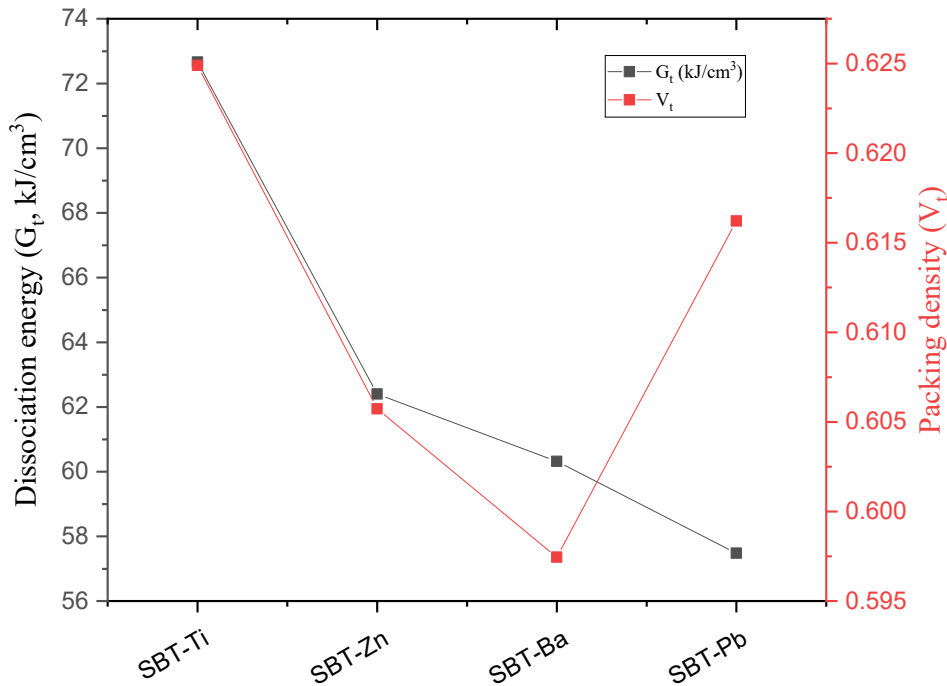


Figure 3. The relationship among the dissociation energy ( $G_t$ ) and packing density ( $V_t$ ) of the fabricated SBT glasses.

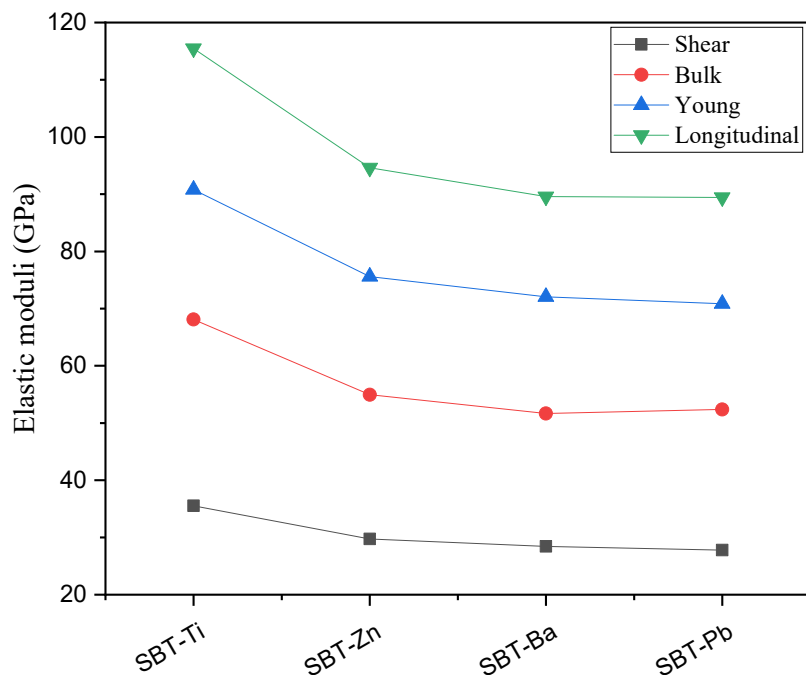
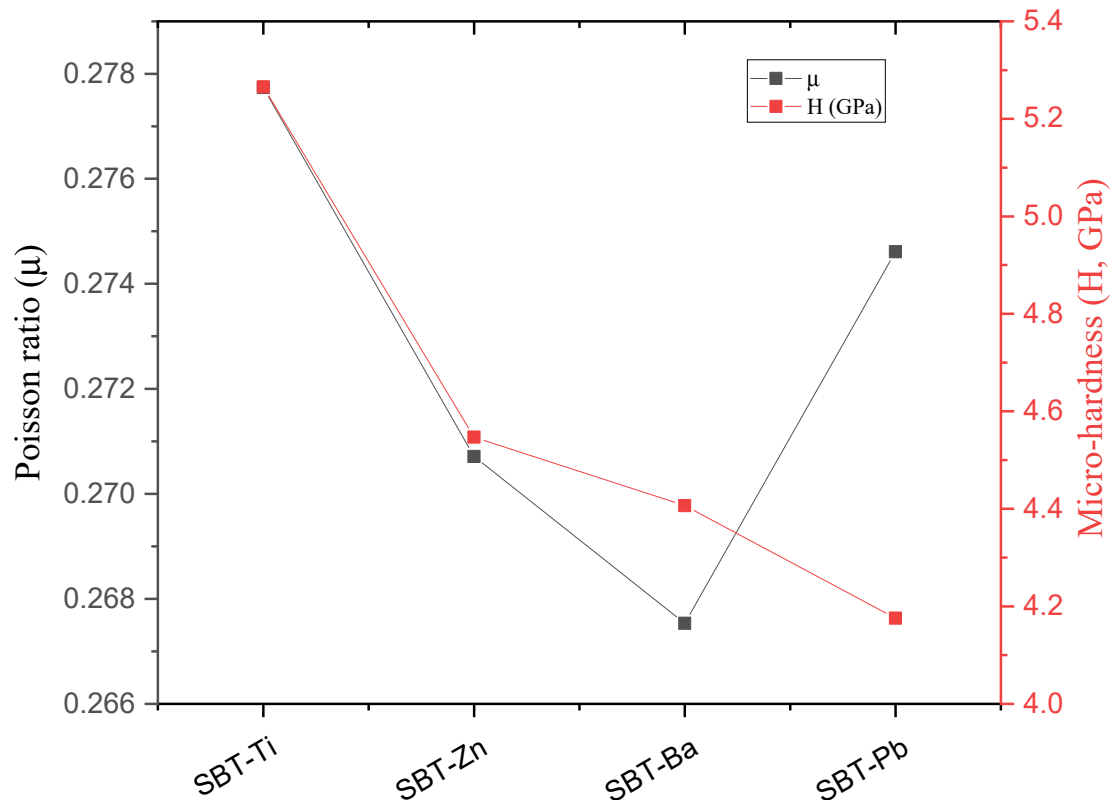


Figure 4. The relationship among the various elastic moduli of the fabricated SBT glasses.



**Figure 5.** The correlation between Poisson ratio ( $\mu$ ) and micro-hardness (H) of the fabricated SBT glasses.

### 3.2. Radiation Attenuation Studies

The mass attenuation coefficient ( $\mu_m$ ,  $\text{cm}^2/\text{g}$ ) of the fabricated SBT-n glasses was calculated in an energy range varied between 0.015 and 15 MeV using the Monte Carlo simulation with a narrow beam transmission method. The achieved results were affirmed using the XCOM theoretical program [34] calculated data for the fabricated sample. Figure 6 shows an agreement between the simulated  $\mu_m$  using MC simulation and the calculated data by the XCOM program, along with the studied energy range. Also, Figure 6 shows that the highest  $\mu_m$  values achieved at gamma-ray energy 0.015 due to the photoelectric interaction, which has a cross-section of interaction that varies inversely with the third power of energy ( $\sigma_{pe} \propto E^{-3.5}$ ). The represented values in Figure 6 showed that the  $\mu_m$  at 0.015 MeV varied in the order of 26.836, 33.419, 35.071, and 52.658  $\text{cm}^2/\text{g}$  for glasses SBT-Ti, SBT-Zn, SBT-Ba, SBT-Pb, respectively. The high variation in the  $\mu_m$  values is related to the significant variation which occurred in the glass samples with the addition of the dopant compounds where the addition of the PbO to SBT glass causes a higher increase in the molecular weight of the fabricated glass, which has a positive effect on the density and atomic weight of the fabricated glasses. Thus, the linear and mass attenuation coefficients are highly increased compared to those glasses doped with  $\text{TiO}_2$ , ZnO, and BaO. The effect of glasses' atomic weight and density appears in the low energy region (photoelectric region) because the cross-section varies directly with the fourth power of the effective atomic number of the glass sample ( $\sigma_{pe} \propto Z^{4-5}$ ) [35,36]. According to the data presented in Figure 6, another interaction region (Compton scattering) began from 0.15 MeV and extended to lower than 5 MeV. In the mentioned region, the variation of the  $\mu_m$  reduced linearly with energy. It linearly increased with the Z. The  $\mu_m$  values varied between 0.3709–0.0311, 0.3853–0.0314, 0.04784–0.0324, and 0.8982–0.0348  $\text{cm}^2/\text{g}$  with an average of 0.1040, 0.1060, 0.1198, 1855  $\text{cm}^2/\text{g}$  for samples SBT-Ti, SBT-Zn, SBT-Ba, SBT-Pb, respectively. Also, the effect of the doping compounds in this energy hasn't a significant

effect compared to the photoelectric region. In the mentioned intermediate region, the linear variation of the  $\mu_m$  values is related to the Compton scattering cross-section where  $CS \propto Z/E$ . In the high energy region ( $E \geq 5$  MeV), according to data presented in Figure 6, the  $\mu_m$  values began to increase with energy increase slightly. This behavior is due to the pair production interaction (PP) in which the cross-section varied with  $\log E$  and  $Z^2$ . Thus, the  $\mu_m$  values are close together for all fabricated samples and they are independent on the incident gamma-ray energy. In this energy region the  $\mu_m$  values have a slight increase between 0.0296–0.0308, 0.0302–0.0318, 0.0319–0.0346, 0.0351–0.0392  $\text{cm}^2/\text{g}$  for the fabricated samples SBT-Ti, SBT-Zn, SBT-Ba, SBT-Pb, respectively.

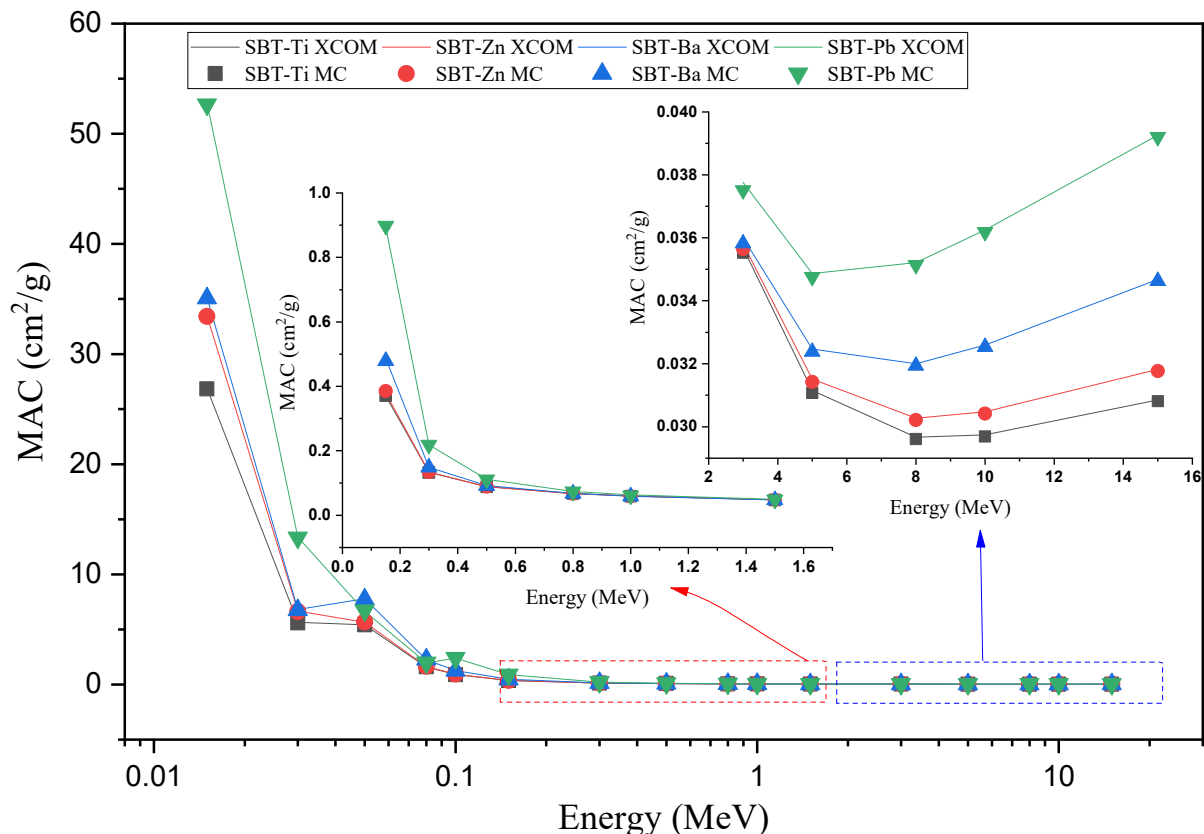


**Figure 6.** Variation of the mass attenuation coefficient versus the gamma-ray energy at different interaction regions.

The relation between the half-value layer (HVL, cm) (the thickness required to reduce the incident gamma flux to half of its initial value [37]) and the incident gamma-ray photons was illustrated in Figure 7. The thinner HVL achieved at the lowest gamma-ray energy among the studied energy range (i.e., 0.015 MeV) takes values 0.006, 0.005, 0.004, and 0.002 for samples SBT-Ti, SBT-Zn, SBT-Ba, and SBT-Pb, respectively. This low value is due to the predominant of the PE interaction at the mentioned energy. Thus, the photon energy is absorbed in one collision with a boundary electron. Also, it is clear that the SBT-Pb has a thinner HVL compared to other fabricated glass samples. This is related to the PbO compound, which has a high density and cross-section of interaction. Hence, insertion of the PbO offers an additional resistance for passing photons, and the result is a significant reduction in the HVL values. In the low energy region in which the PE interaction is predominant, the HVL suffers a high increase with raising the photon energy. Increasing the energy of incident photons higher than 0.1 MeV causes a change in the interaction mode in which gamma-ray interacts with the glass atoms, where the PE decreases and CS begins to increase with raising the incident gamma photon energies. In this energy interval, the HVL increased linearly with energy. The HVL varies the range of 0.191–3.588, 0.171–3.397, 0.114–3.117, 0.054–2.717 cm with average HVL of 1.844, 1.739, 1.546, and 1.234 cm for glass samples SBT-Ti, SBT-Zn, SBT-Ba, SBT-Pb, respectively. The HVL continued its increase

with the incident energy until 5 MeV, and then it began to reverse the trend and decreased slightly with raising the incident gamma photon energy. This decrease is due to the pair production, as illustrated in the mass attenuation coefficient section. The HVL in the mentioned interval varied between 5.768–5.543, 5.340–5.078, 4.579–4.223, 3.746–3.358 cm for samples SBT-Ti, SBT-Zn, SBT-Ba, SBT-Pb when the incident energy varied between 8 and 15 MeV, respectively.

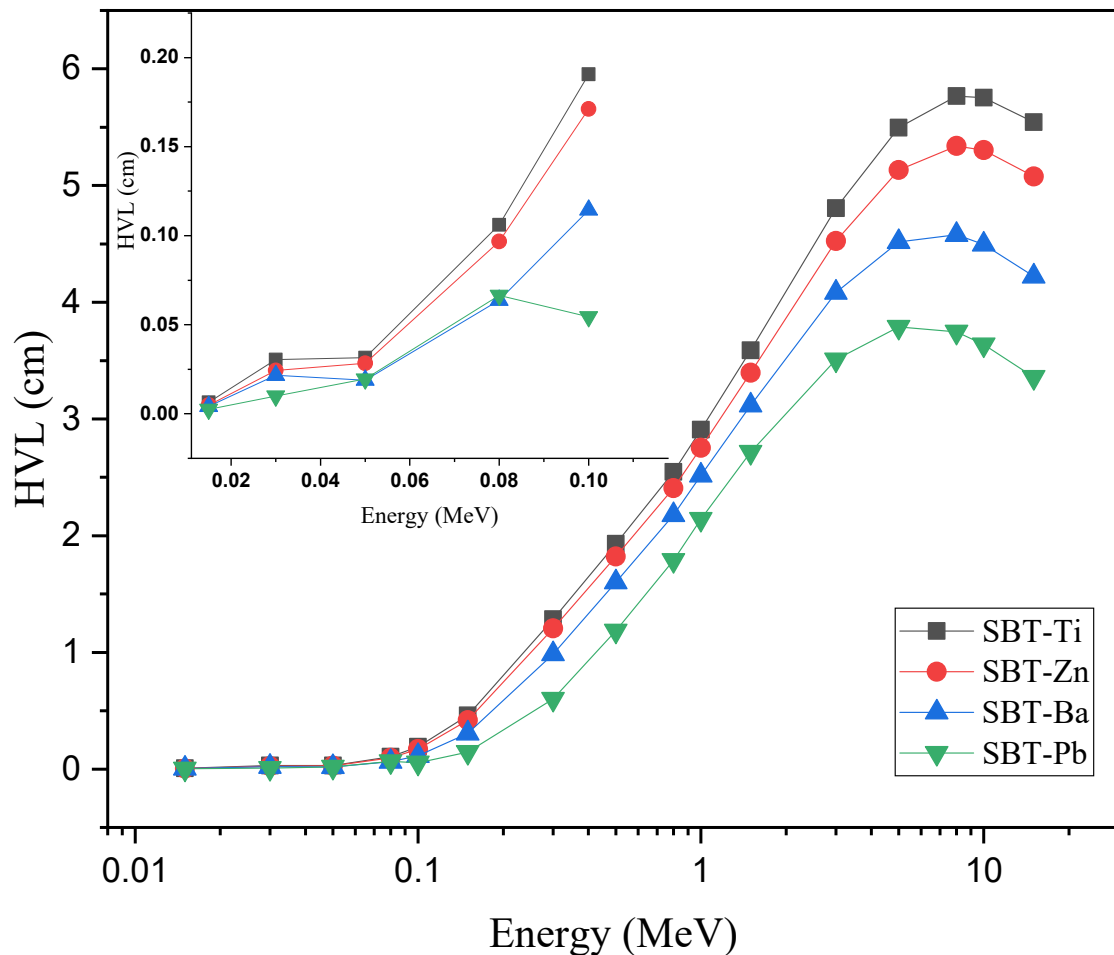


**Figure 7.** Variation of the half-value layer (cm) versus the gamma-ray energy for the fabricated SBT glasses.

The fabricated glasses' thickness ( $D_{eq}$ ) equivalent to 1 cm of lead (Pb) was calculated at various energies, as presented in Figure 8. For all samples except the SBT-Pb, the  $D_{eq}$  start very high at low energy. It takes values of 11.62, 8.81, 7.61, 4.56 cm for glasses SBT-Ti, SBT-Zn, SBTBa, and SBT-Pb, respectively. This high value of  $D_{eq}$  is related to the high linear attenuation coefficient (LAC) of the Pb standard sample, where the LAC of the fabricated glasses is low compared to the LAC of Pb. After that, a sharp drop was achieved between 0.05 and 0.08 MeV. This reduction in the  $D_{eq}$  for all samples is related to the K absorption edges of Te, which is the glass former in all studied glasses. In this energy interval between 0.05 and 0.08 MeV the  $D_{eq}$  takes values of 4.14, 3.73, 2.49, and 2.57 cm for samples SBT-Ti, SBT-Zn, SBTBa, and SBT-Pb. Above 0.1 MeV, the  $D_{eq}$  began to decrease gradually with increasing the incident gamma-ray energy. This is due to the CS interaction and increases in the LAC of fabricated glasses compared to Pb in this energy region. The lowest values of  $D_{eq}$  achieved at gamma-ray energy, 1.5 MeV, take values 3.07, 2.90, 2.66, and 2.32 cm for the fabricated glasses SBT-Ti, SBT-Zn, SBTBa, and SBT-Pb. This illustrates that the fabricated glasses have a shielding capacity varied between 30 and 43% compared to the pure Pb at gamma-ray energy of 1.5 MeV. Above 1.5 MeV, the  $D_{eq}$  began to increase slightly due to the

small increase in the LAC of Pb compared to the fabricated glass samples. Also, Figure 8 illustrates that the high values of  $D_{eq}$  obtained for glass samples SBT-Ti while the lowest achieved for the SBT-Pb. This is related to the amount of gamma-ray passing resistance offered by  $TiO_2$  and  $PbO$  compounds, where the mentioned resistance for  $PbO$  is higher than that of  $TiO_2$ . Thus, the linear attenuation coefficient of the glasses containing  $PbO$  is higher than that of  $TiO_2$  glasses, and the  $D_{eq}$  for  $PbO$  doped glasses is lower than that of  $TiO_2$  doped glasses.

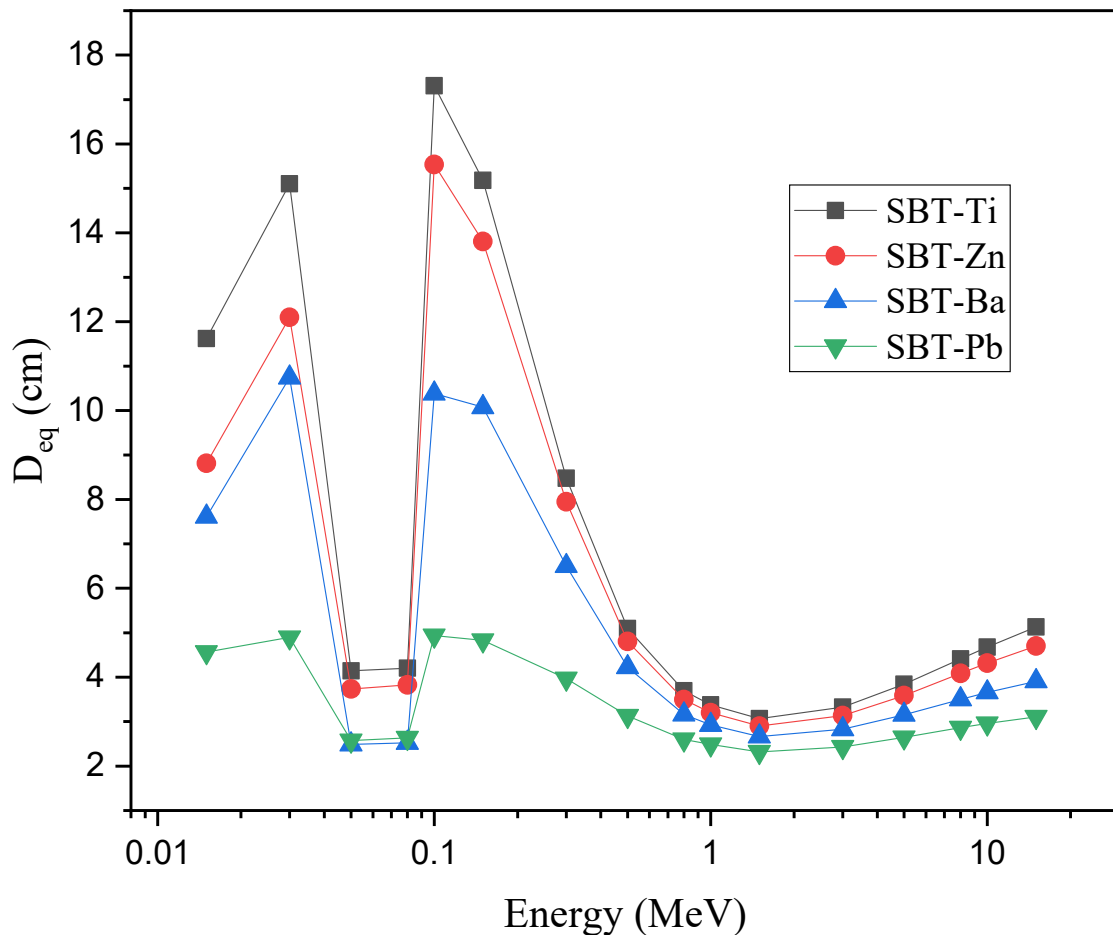


**Figure 8.** The samples' thickness equal to 1 cm of lead at different gamma-ray energy.

The transmission factor (TF, %) measures the photon numbers that can penetrate or escape from the shielding material. In contrast, the radiation protection efficiency (RPE, %) measures the number of photons that the shielding material can stop or absorb during the interaction. Both TF and RPE were investigated for the fabricated glasses and presented in Figure 9 versus the incident gamma-ray photon. Figure 9a shows that the TF values at low gamma-ray energy up to 0.1 MeV are very small due to the photoelectric interaction, which consumes the low energy of photons totally in the interaction to produce a free electron. As a result, the photon is absorbed inside the fabricated SBT-n glasses, and the probability of scattering or escaping photons from the fabricated materials is very low. Thus, the TF values tend to be minimum values. With increasing the incident gamma-ray energy, some photons began to pass enough energy to penetrate and transmit the fabricated material. This is due to the change in the photon interaction mode where the photoelectric interaction decreases and the Compton scattering interaction begins to be the dominant interaction. Hence, the scattering and penetrated photons increase. The TF values increase gradually with increasing the CS interaction until maximum values at 8 MeV. The TF values for a thickness of 1 cm of the fabricated samples reach 88.68, 87.83, 85.95, and 83.11% for

glasses SBT-Ti, SBT-Zn, SBT-Ba, and SBT-Pb, respectively. After that, a slight decrease in the TF values was observed when the photon energy raised above 8 MeV due to the pair production interaction in which the probability of photon annihilation increased when the photon energy increased more than 1.024 MeV.

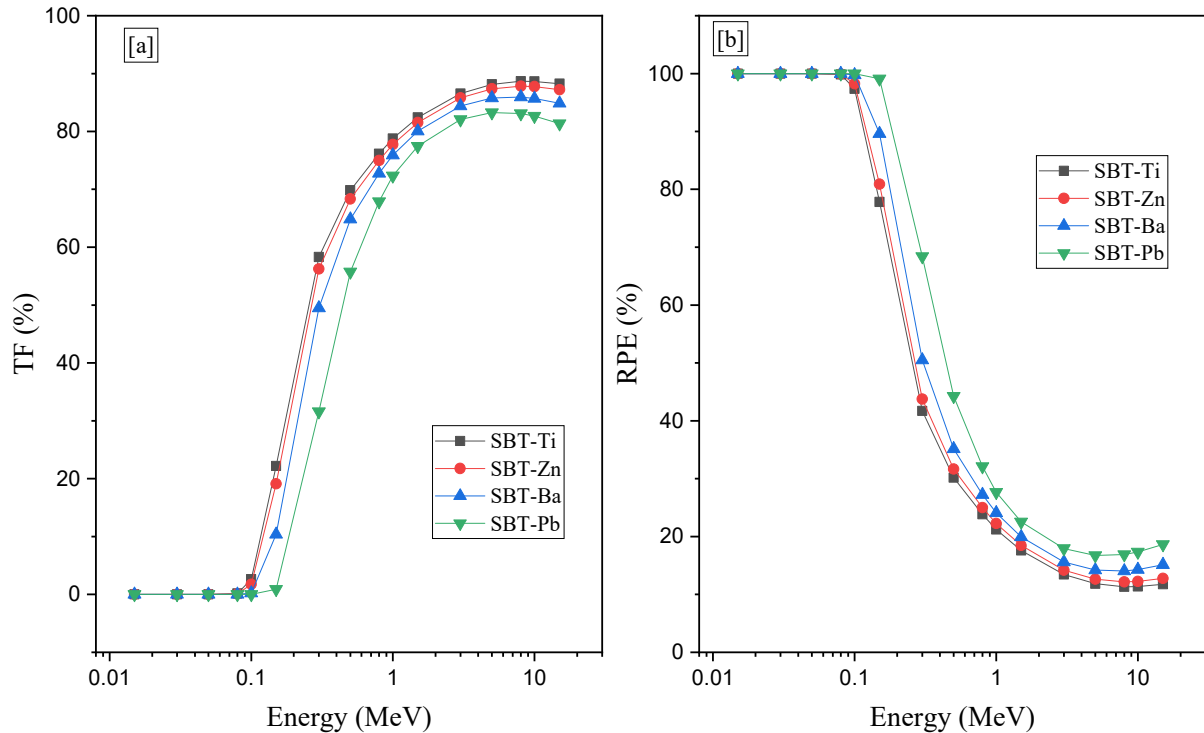


**Figure 9.** (a) Variation of the transmission factor (TF) and (b) the radiation protection efficiency (RPE) versus the gamma-ray energy.

In contrast, Figure 9b illustrates the RPE variation versus the incident gamma photon energies, where the first look demonstrates that the RPE is totally opposite to the TF. The RPE at low energy is close to 100% because of the high absorption cross-section of the fabricated glasses for the low-energy photons. Thus, all photons with energy lower than 0.15 MeV are absorbed inside the glass layer and can't penetrate a thickness of 1 cm of the fabricated glass samples. Above 0.15 MeV, the scattered photons from the fabricated glass thickness increased, and the number of photons penetrating the thickness began to increase with photon energy. Thus, the RPE reduced gradually with energy until minimum RPE was achieved at 8 MeV. The minimum RPE is 11.32, 12.17, 14.05, and 16.89% for samples SBT-Ti, SBT-Zn, SBT-Ba, and SBT-Pb, respectively.

Figure 10 illustrates the effect of glass thickness on the TF and RPE values. It is clear that from Figure 10a, the TF decreases gradually with growing the glass thickness where the TF values reduced between 88.76 and 30.36% (for SBT-Ti), 77.74 and 28.39% (for SBT-Zn), 75.93 and 25.239% (for SBT-Ba), 72.353 and 19.819% (for SBR-Pb) when the glass thickness grow between 0.5 and 4 cm, respectively, for gamma-ray energy of 1 MeV. Raising the glass thickness increases the probability of gamma-ray interaction along their path length. Thus, the photon loses a high amount of its energies in collisions and does not have enough power to penetrate the material thickness. As a result, the TF values decrease with growing the fabricated glasses thickness.

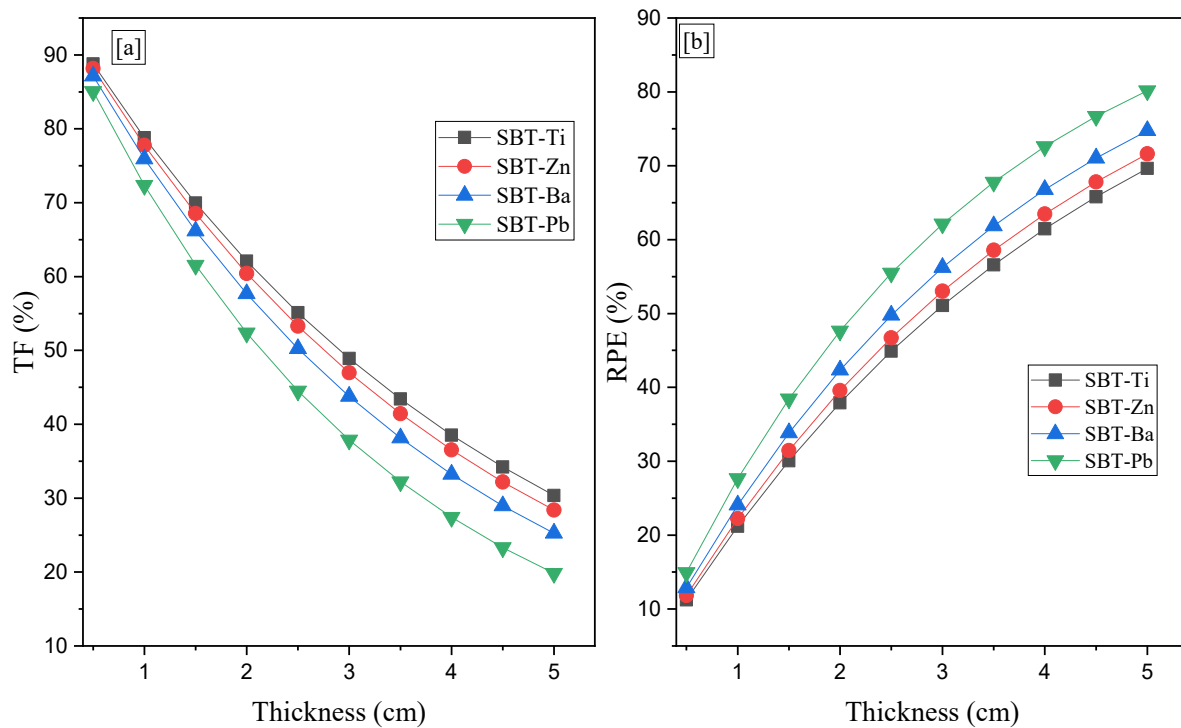


**Figure 10.** (a) Variation of the transmission factor (TF) and (b) the radiation protection efficiency (RPE) versus the SBT glasses thickness.

In contrast, the RPE increases gradually with growing the fabricated glass thickness, as illustrated in Figure 10b. The mentioned figure showed that the low values of RPE achieved at the thinner thicknesses are related to the TF of the gamma photons. For thinner thicknesses, the photons TF is relatively high, so a lot of photons can penetrate the shielding thickness and reach the human cells beyond the shielding. Thus, the RPE offered by this shielding thickness is relatively low. With growing the glass thickness, the TF decreases, as mentioned earlier, so the number of photons penetrating the thickness becomes small, and the RPE increases. At gamma-ray energy of 1 MeV, the RPE increases between 11.23–69.63%, 11.82–71.60%, 12.86–74.76%, and 14.93–80.17% for the fabricated glass samples SBT-Ti, SBT-Zn, SBT-Ba, and SBT-Pb, respectively.

#### 4. Conclusions

Boro-tellurate glasses were fabricated using four various modifier oxides and investigated the influence of these oxides on both the mechanical and radiation shielding properties of the prepared samples. Monte Carlo simulation and the Makishima-Mackenzie model have been used in this work. The linear and mass attenuation coefficients for the glass with PbO are higher than the other samples. Thus, the SBT-Pb glass sample has a better attenuation competence than the SBT-Ti, SBT-Zn, and SBT-Ba samples. The thinner HVL achieved at the lowest gamma-ray energy among the studied energy range (i.e., 0.015 MeV) takes values 0.006, 0.005, 0.004, and 0.002 for samples SBT-Ti, SBT-Zn, SBT-Ba, and SBT-Pb, respectively. At moderate energy, the HVL varies the range of 0.191–3.588, 0.171–3.397, 0.114–3.117, 0.054–2.717 cm with average HVL of 1.844, 1.739, 1.546, and 1.234 cm for glass samples SBT-Ti, SBT-Zn, SBT-Ba, SBT-Pb, respectively. While the HVL in the high energy region varied between 5.768–5.543, 5.340–5.078, 4.579–4.223, 3.746–3.358 cm for samples SBT-Ti, SBT-Zn, SBT-Ba, SBT-Pb. At 1 MeV, the RPE increases between 11.23–69.63%, 11.82–71.60%, 12.86–74.76%, and 14.93–80.17% for the fabricated glass samples SBT-Ti, SBT-Zn, SBT-Ba, and SBT-Pb, respectively. The TF and RPE results reaffirm that utilization of the PbO in the prepared glasses has a considerable role in the attenuation performance for the prepared samples.

**Author Contributions:** M.I.S.: Software; investigation, writing—review and editing, M.K.H.: Conceptualization; investigation, writing—review and editing, M.H.A.M.: Methodology; investigation, writing—review and editing, K.A.N.: Formal analysis, writing—original draft preparation, K.A.M.: Validation; resources; data curation, writing—review and editing, M.U.K.: Writing—original draft preparation, supervision, H.O.: Funding acquisition, project administration, B.H.E.: Supervision, funding acquisition. All authors have read and agreed to the published version of the manuscript.

**Funding:** The authors acknowledge the support of Taif University Researchers Supporting Project number (TURSP-2020/127), Taif University, Taif, Saudi Arabia.

**Institutional Review Board Statement:** Not applicable.

**Informed Consent Statement:** Not applicable.

**Data Availability Statement:** Not Applicable.

**Conflicts of Interest:** The authors declare no conflict of interest.

## References

1. Akkurt, I.; Basyigit, C.; Kilincarslan, S.; Mavi, B. The shielding of  $\gamma$ -rays by concretes produced with barite. *Prog. Nucl. Energy* **2005**, *46*, 1–11. [[CrossRef](#)]
2. Xu, S.; Bourham, M.; Rabiei, A. A novel ultra-light structure for radiation shielding. *Mater. Des.* **2010**, *31*, 2140–2146. [[CrossRef](#)]
3. Olukotun, S.; Gbenu, S.; Ibitoye, F.; Oladejo, O.; Shittu, H.; Fasasi, M.; Balogun, F. Investigation of gamma radiation shielding capability of two clay materials. *Nucl. Eng. Technol.* **2018**, *50*, 957–962. [[CrossRef](#)]
4. Harrison, C.; Weaver, S.; Bertelsen, C.; Burgett, E.; Hertel, N.; Grulke, E. Polyethylene/boron nitride composites for space radiation shielding. *J. Appl. Polym. Sci.* **2008**, *109*, 2529–2538. [[CrossRef](#)]
5. Mahmoud, K.A.; Tashlykov, O.L.; Mhareb, M.; Almuqrin, A.H.; Alajerami, Y.; Sayyed, M. A new heavy-mineral doped clay brick for gamma-ray protection purposes. *Appl. Radiat. Isot.* **2021**, *173*, 109720. [[CrossRef](#)] [[PubMed](#)]
6. Oto, B.; Yıldız, N.; Akdemir, F.; Kavaz, E. Investigation of gamma radiation shielding properties of various ores. *Prog. Nucl. Energy* **2015**, *85*, 391–403. [[CrossRef](#)]
7. Çelen, Y.Y.; Evcin, A. Synthesis and characterizations of magnetite-borogypsum for radiation shielding. *Emerg. Mater. Res.* **2020**, *9*, 770–775. [[CrossRef](#)]
8. Sayyed, M.; Abdalsalam, A.H.; Taki, M.M.; Mhareb, M.; Alim, B.; Baltakesmez, A.; Şakar, E. MoO<sub>3</sub> reinforced Ultra high molecular weight PE for neutrons shielding applications. *Radiat. Phys. Chem.* **2020**, *172*, 108852. [[CrossRef](#)]
9. Alajerami, Y.S.M.; Morsy, M.A.; Mhareb, M.H.A.; Sayyed, M.I.; Imheidat, M.A.; Hamad, M.K.; Karim, M.K.A. Structural, optical, and radiation shielding features for a series of borate glassy system modified by molybdenum oxide. *Eur. Phys. J. Plus* **2021**, *136*, 1–18. [[CrossRef](#)]
10. Mhareb, M.; Alqahtani, M.; Alshahri, F.; Alajerami, Y.; Saleh, N.; Alonizan, N.; Sayyed, M.; Ashiq, M.; Ghrib, T.; Al-Dhafar, S.I.; et al. The impact of barium oxide on physical, structural, optical, and shielding features of sodium zinc borate glass. *J. Non-Cryst. Solids* **2020**, *541*, 120090. [[CrossRef](#)]
11. Naseer, K.; Marimuthu, K.; Al-Buriahi, M.; Alalawi, A.; Tekin, H. Influence of Bi<sub>2</sub>O<sub>3</sub> concentration on barium-telluro-borate glasses: Physical, structural and radiation-shielding properties. *Ceram. Int.* **2020**, *47*, 329–340. [[CrossRef](#)]
12. Libeesh, N.; Naseer, K.; Arivazhagan, S.; El-Rehim, A.A.; Mahmoud, K.; Sayyed, M.; Khandaker, M.U. Advanced nuclear radiation shielding studies of some mafic and ultramafic complexes with lithological mapping. *Radiat. Phys. Chem.* **2021**, *189*, 109777. [[CrossRef](#)]
13. Mhareb, M.; Alsharhan, R.; Sayyed, M.; Alajerami, Y.; Alqahtani, M.; Alayed, T.; Almurayshid, M. The impact of TeO<sub>2</sub> on physical, structural, optical and radiation shielding features for borate glass samples. *Optik* **2021**, *247*, 167924. [[CrossRef](#)]
14. Dwaikat, N.; Sayyed, M.; Mhareb, M.; Dong, M.; Alajerami, Y.; Alrammah, I.; Khalid, A.; Ashiq, M. Durability, optical and radiation shielding properties for new series of boro-tellurite glass. *Optik* **2021**, *245*, 167667. [[CrossRef](#)]
15. Naseer, K.A.; Karthikeyan, P.; Arunkumar, S.; Suthanthirakumar, P.; Marimuthu, K. Enhanced luminescence properties of Er<sup>3+</sup>/Yb<sup>3+</sup> doped zinc tellurofluoroborate glasses for 1.5  $\mu$ m optical amplification. *AIP Conf. Proc.* **2020**, *2265*, 030237. [[CrossRef](#)]
16. Naseer, K.; Arunkumar, S.; Marimuthu, K. The impact of Er<sup>3+</sup> ions on the spectroscopic scrutiny of Bismuth bariumtelluroborate glasses for display devices and 1.53  $\mu$ m amplification. *J. Non-Cryst. Solids* **2019**, *520*, 119463. [[CrossRef](#)]
17. Naseer, K.; Marimuthu, K. The impact of Er/Yb co-doping on the spectroscopic performance of bismuth borophosphate glasses for photonic applications. *Vacuum* **2020**, *183*, 109788. [[CrossRef](#)]
18. Chen, Q.; Naseer, K.A.; Marimuthu, K.; Kumar, P.S.; Miao, B.; Mahmoud, K.A.; Sayyed, M.I. Influence of modifier oxide on the structural and radiation shielding features of Sm<sup>3+</sup>-doped calcium telluro-fluoroborate glass systems. *J. Aust. Ceram. Soc.* **2021**, *57*, 275–286. [[CrossRef](#)]
19. Suthanthirakumar, P.; Arunkumar, S.; Marimuthu, K. Investigations on the spectroscopic properties and local structure of Eu<sup>3+</sup> ions in zinc telluro-fluoroborate glasses for red laser applications. *J. Alloy. Compd.* **2018**, *760*, 42–53. [[CrossRef](#)]

20. Mhareb, M.; Alajerami, Y.; Sayyed, M.; Dwaikat, N.; Alqahtani, M.; Alshahri, F.; Saleh, N.; Alonizan, N.; Ghrib, T.; Al-Dhafar, S.I. Radiation shielding, structural, physical, and optical properties for a series of borosilicate glass. *J. Non-Cryst. Solids* **2020**, *550*, 120360. [[CrossRef](#)]
21. Krause, S.; Pfau, C.; Dyrba, M.; Miclea, P.-T.; Schweizer, S. On the role of the network modifier PbO in Sm<sup>3+</sup>-doped borate glasses. *J. Lumin.* **2014**, *151*, 29–33. [[CrossRef](#)]
22. Hamad, M.K.; Mhareb, M.H.A.; Alajerami, Y.S.; Sayyed, M.I.; Saleh, G.; Maswadeh, Y.; Ziq, K. Radiation shielding properties of Nd<sub>0.6</sub>Sr<sub>0.4</sub>Mn<sub>1-y</sub>NiyO<sub>3</sub> substitute with different concentrations of nickle. *Radiat. Phys. Chem.* **2020**, *174*, 108920. [[CrossRef](#)]
23. Hamad, R.M.; Mhareb, M.H.A.; Alajerami, Y.S.; Sayyed, M.I.; Saleh, G.; Hamad, M.K.; Ziq, K. A comprehensive ionizing radiation shielding study of FexSe<sub>0.5</sub>Te<sub>0.5</sub> alloys with various iron concentrations. *J. Alloys Compd.* **2021**, *858*, 157636. [[CrossRef](#)]
24. Makishima, A.; MacKenzie, J. Direct calculation of Young's modulus of glass. *J. Non-Cryst. Solids* **1973**, *12*, 35–45. [[CrossRef](#)]
25. Makishima, A.; MacKenzie, J.D. Calculation of bulk modulus, shear modulus and Poisson's ratio of glass. *J. Non-Cryst. Solids* **1975**, *17*, 147–157. [[CrossRef](#)]
26. El-Moneim, A.A. Effect of ZnF<sub>2</sub> and WO<sub>3</sub> on elastic properties of oxyfluoride tellurite ZnF<sub>2</sub>-WO<sub>3</sub>-TeO<sub>2</sub> glasses: Theoretical analysis. *Chin. J. Phys.* **2020**, *65*, 412–423. [[CrossRef](#)]
27. X-5 Monte Carlo Team. *MCNP—A General Monte Carlo N-Particle Transport Code; Version 5; La-Ur-03-1987, II; MCNP: Punjab, India, 2003.*
28. Naseer, K.A.; Marimuthu, K.; Mahmoud, K.A.; Sayyed, M.I. Impact of Bi<sub>2</sub>O<sub>3</sub> modifier concentration on barium-zincborate glasses: Physical, structural, elastic, and radiation-shielding properties. *Eur. Phys. J. Plus* **2021**, *136*, 116. [[CrossRef](#)]
29. Teresa, P.E.; Naseer, K.; Marimuthu, K.; Alavian, H.; Sayyed, M. Influence of modifiers on the physical, structural, elastic and radiation shielding competence of Dy<sup>3+</sup> ions doped Alkali boro-tellurite glasses. *Radiat. Phys. Chem.* **2021**, *189*, 109741. [[CrossRef](#)]
30. Kurtuluş, R.; Kavas, T.; Agar, O.; Turhan, M.; Kaçal, M.; Dursun, I.; Akman, F. Study on recycled Er-incorporated waste CRT glasses for photon and neutron shielding. *Ceram. Int.* **2021**, *47*, 26335–26349. [[CrossRef](#)]
31. Saddeek, Y.B.; El Latif, L. Effect of TeO<sub>2</sub> on the elastic moduli of sodium borate glasses. *Phys. B Condens. Matter* **2004**, *348*, 475–484. [[CrossRef](#)]
32. Hager, I. Effect of Er<sub>2</sub>O<sub>3</sub> and ErF<sub>3</sub> on the structural and elastic properties of sodium oxyfluoroborate glasses. *J. Alloy. Compd.* **2012**, *539*, 256–263. [[CrossRef](#)]
33. Gerward, L.; Guilbert, N.; Jensen, K.B.; Levring, H. X-ray absorption in matter. Reengineering XCOM. *Radiat. Phys. Chem.* **2001**, *60*, 23–24. [[CrossRef](#)]
34. Yasmin, S.; Barua, B.S.; Khandaker, M.U.; Rashid, M.A.; Bradley, D.A.; Olatunji, M.A.; Kamal, M. Studies of ionizing radiation shielding effectiveness of silica-based commercial glasses used in Bangladeshi dwellings. *Results Phys.* **2018**, *9*, 541–549. [[CrossRef](#)]
35. Yasmin, S.; Rozaila, Z.S.; Khandaker, M.U.; Barua, B.S.; Chowdhury, F.U.Z.; Rashid, M.A.; Bradley, D.A. The radiation shielding offered by the commercial glass installed in Bangladeshi dwellings. *Radiat. Eff. Defects Solids* **2018**, *173*, 657–672. [[CrossRef](#)]
36. Dong, M.; Xue, X.; Yang, H.; Li, Z. Highly cost-effective shielding composite made from vanadium slag and boron-rich slag and its properties. *Radiat. Phys. Chem.* **2017**, *141*, 239–244. [[CrossRef](#)]
37. Dong, M.; Xue, X.; Yang, H.; Liu, D.; Wang, C.; Li, Z. A novel comprehensive utilization of vanadium slag: As gamma ray shielding material. *J. Hazard. Mater.* **2016**, *318*, 751–757. [[CrossRef](#)] [[PubMed](#)]